nature chemistry

ARTICLES

PUBLISHED ONLINE: 19 SEPTEMBER 2010 | DOI: 10.1038/NCHEM.828

Synthesis of polyynes to model the *sp*-carbon allotrope carbyne

Wesley A. Chalifoux and Rik R. Tykwinski[†]*

Carbyne is an allotrope of carbon composed of *sp*-hybridized carbon atoms. Although its formation in the laboratory is suggested, no well-defined sample is described. Interest in carbyne and its potential properties remains intense because of, at least in part, technological breakthroughs offered by other carbon allotropes, such as fullerenes, carbon nanotubes and graphene. Here, we describe the synthesis of a series of conjugated polyynes as models for carbyne. The longest of the series consists of 44 contiguous acetylenic carbons, and it maintains a framework clearly composed of alternating single and triple bonds. Spectroscopic analyses for these polyynes reveal a distinct trend towards a finite gap between the highest occupied molecular orbital and the lowest unoccupied molecular orbital for carbyne, which is estimated to be ∼485 nm (∼2.56 eV). Even the longest members of this series of polyynes are not particularly sensitive to light, moisture or oxygen, and they can be handled and characterized under normal laboratory conditions.

By mass, carbon is the fourth most-abundant element in the universe, and it is essential to all known forms of life[1]. In terms of naturally occurring carbon, typically two forms (allotropes) are encountered, namely diamond (sp^3-hybridized carbon) and graphite (sp^2-hybridized carbon). In each case, it is the bulk properties of these allotropes that are of interest, properties that differ quite dramatically for each allotropic form. For example, diamond is the hardest known naturally occurring material and also a good electrical insulator. Graphite, however, is much softer and shows high conductivity[2]. Carbon allotropes discovered more recently, such as fullerenes, nanotubes and graphene (all composed of sp^2-hybridized carbon) each also show unique properties, often different from those of either diamond or graphite, and they offer the promise of technological breakthroughs[3].

Next in the series of carbon-atom hybridization from sp^3- to sp^2- is *sp*-hybridization and the least well-known of the carbon allotropes, carbyne (Fig. 1). Whereas diamond and graphite feature an atomic carbon skeleton with covalent bonding in three and two dimensions, respectively, carbyne is expected to feature a linear or approximately linear one-dimensional framework. Carbyne is proposed to exist in interstellar dust[4], meteorites[5] and as a by-product of shock-fused graphite[6]. There are reports of the laboratory formation of carbyne by a number of routes, including gas-phase deposition techniques, electrochemical synthesis, dehydrohalogenation of polymers and others[7,8]. In all these cases, the resulting product or material is ill-defined, and the specific properties of carbyne thus remains unrealized.

In the absence of a well-defined or indisputable sample of carbyne, synthetic chemists addressed the question of its potential properties through the formation of homologous series of polyyne molecules (Fig. 1)[9]. More specifically, this involved the synthesis of oligomers of defined length and composed only of acetylenic segments that are end-capped with a sterically bulky group designed to stabilize the polyyne chain. For a particular set of oligomers, convergence of spectroscopic data versus length to a constant value (saturation) can be evaluated to shed light on the expected properties of the polymer carbyne. A notable example is that of the triethylsilyl end-capped series **TES[*n*]** (Fig. 1), which provided isolable samples for $n = 6$ and 8 (ref. 10). The attempted synthesis of longer derivatives, however, gave **TES[10]**, **TES[12]** and **TES[16]**, which could be manipulated only in solution, but the longest molecule, **TES[16]**, could not be purified[10]. Polyynes **Pt[*n*]** were isolated and characterized up to $n = 14$; **Pt[14]** is the longest isolable polyyne reported to date[11].

Recognizing that large, sterically demanding end-capping groups should provide synthetic access to much longer polyynes, we used the tris(3,5-di-*t*-butylphenyl)methyl moiety (Tr*, Fig. 1)[12] and report here the synthesis of polyynes with unprecedented length: the series **1a**–**1j** is composed of polyynes of up to $n = 22$ acetylenic bonds (that is, 44 contiguous *sp*-carbons). Structure–property analyses for polyynes **1a**–**1j** provide predictions as to the highest occupied molecular orbital (HOMO)–lowest unoccupied molecular orbital (LUMO) gap and structure of carbyne.

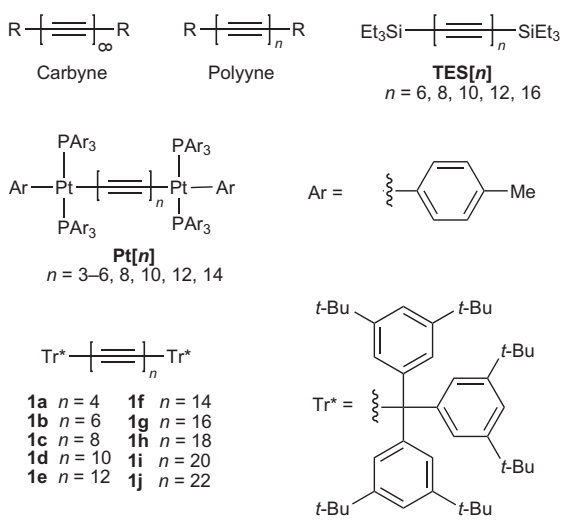

Figure 1 | Schematic structures of carbyne, polyyne and several polyyne species.

Department of Chemistry, University of Alberta, Edmonton, Alberta, T6G 2G2 Canada; [†]Present address: Institut für Organische Chemie, Friedrich-Alexander-Universität, Erlangen-Nürnberg, Henkestrasse 42, 91054 Erlangen, Germany. *e-mail: rik.tykwinski@chemie.uni-erlangen.de

Table 1 | Synthesis of polyynes 4e–4k (c = 5–11).

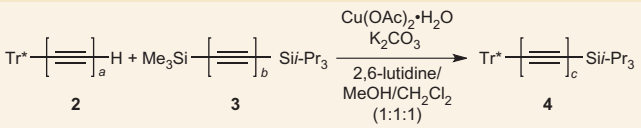

Entry	Substrate 2	Substrate 3	4, % yield
1	**2b** (a = 2)	**3c** (b = 3)	**4e** (c = 5), 84
2	**2c** (a = 3)	**3c** (b = 3)	**4f** (c = 6), 63
3	**2c** (a = 3)	**3d** (b = 4)	**4g** (c = 7), 73
4	**2d** (a = 4)	**3d** (b = 4)	**4h** (c = 8), 77
5	**2e** (a = 5)	**3d** (b = 4)	**4i** (c = 9), 42
6	**2f** (a = 6)	**3d** (b = 4)	**4j** (c = 10), 52
7	**2g** (a = 7)	**3d** (b = 4)	**4k** (c = 11), 35

Table 2 | Synthesis of polyynes 1a–1j (n = 4–22).

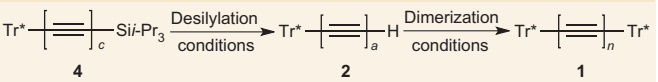

4	2, yield, %	1, yield, %
–	**2b** (a = 2)†	**1a** (n = 4), 92¶
4c (c = 3)*	**2c** (a = 3), 91‡	**1b** (n = 6), 66¶
4d (c = 4)*	**2d** (a = 4), 100§	**1c** (n = 8), 97¶
4e (c = 5)	**2e** (a = 5), 99§	**1d** (n = 10), 26#, 74**
4f (c = 6)	**2f** (a = 6), 93§	**1e** (n = 12), 41#, 86**
4g (c = 7)	**2g** (a = 7)§‖	**1f** (n = 14), 90**
4h (c = 8)	**2h** (a = 8)§‖	**1g** (n = 16), 76**
4i (c = 9)	**2i** (a = 9)§‖	**1h** (n = 18), 81**
4j (c = 10)	**2j** (a = 10)§‖	**1i** (n = 20), 57**
4k (c = 11)	**2k** (a = 11)§‖	**1j** (n = 22), 18**

*The synthesis of **4c** and **4d** is described in the Supplementary Information (pp S15–S17). †Diyne **2b** was produced by a different method, see Supplementary Information (pp S12–S13). ‡Desilylation using tetrabutylammonium fluoride, THF, room temperature. §Desilylation using CsF in tetrahydrofuran/H_2O (5:1), room temperature. ‖Product carried on directly to next step. ¶Oxidative dimerization using CuCl, tetramethylethylenediamine, CH_2Cl_2, O_2. #Oxidative dimerization using $Cu(OAc)_2{\cdot}H_2O$ (excess), pyridine, CH_2Cl_2. **Oxidative dimerization using $Cu(OAc)_2{\cdot}H_2O$ (excess), 2,6-lutidine, CH_2Cl_2.

Results and discussion

The formation of the synthetic precursors to polyynes **1a**–**1j** is designed around a chain-extension sequence using the terminal polyynes **2b**–**2g** in a reaction with differentially end-capped polyynes **3c** and **3d**, where a and b represent the number of acetylene units in precursors **2** and **3**, respectively (Table 1). The building blocks **2b**–**2d** and **3c** and **3d** were assembled readily based on reported methods (see Supplementary Information (pp S12–S18) and Jahnke and Tykwinski[13]), and the synthesis of **2e**–**2g** is described below. This chain extension was accomplished efficiently using a modified Eglinton–Galbraith protocol to generate unsymmetrical Tr*–$[C{\equiv}C]_c$–Sii-Pr_3 polyynes (**4e**–**4k**)[14,15]. Specifically, allowing a mixture of the appropriate terminal polyyne **2b**–**2g** (a = 2–7) and either **3c** (b = 3) or **3d** (b = 4) to react in the presence of excess $Cu(OAc)_2{\cdot}H_2O$, K_2CO_3 and 2,6-lutidine resulted in the formation of polyynes **4e**–**4k** in good to moderate yields (Table 1, entries 1–4 and entries 5–7, respectively). Three notable aspects of this process are: (1) removal of the trimethylsilyl groups of **3c** and **3d** was effected *in situ* under the Eglinton–Galbraith reaction conditions, which eliminated the need for an independent desilylation step[16], (2) use of 2,6-lutidine in place of the typical base, pyridine, was essential to the success of the reaction and (c) **4i**, **4j** and **4k** represent the longest unsymmetrical polyynes isolated and characterized to date.

Removal of the terminal i-Pr_3Si groups from polyynes **4c**–**4k** to give terminal polyynes **2c**–**2k** (Table 2) was first explored using tetrabutylammonium fluoride as a desilylation agent at low temperature. Under these conditions **4c** was desilylated successfully, but significant decomposition was observed for longer derivatives. Ultimately, desilylation was achieved using CsF in a 5:1 mixture of tetrahydrofuran (THF)/H_2O, which provided polyynes **2d**–**2k** with little apparent decomposition based on ultraviolet–visible spectroscopic analyses (see Supplementary Fig. S1).

The stabilizing influence of the Tr* end-capping group was already quite evident at this point, in that terminal polyynes up to seven triple bonds in length (**2g**) could be isolated neat and characterized by ^{1}H and ^{13}C NMR, infrared and ultraviolet–visible spectroscopy, as well as by mass spectrometry (although within minutes the terminal polyyne **2g** showed signs of decomposition as a solid). To our knowledge, the longest terminal polyyne previously isolable as a stable, neat solid was a tetrayne[17]. Given the instability observed for **2g** in the solid state, attempts were not made to isolate the longer terminal polyynes **2h**–**2k**. Thus, after formation by desilylation, the products **2g**–**2k**, after work up, were taken on directly to the formation of **1f**–**1j**. Polyynes **2h**–**2k** could, however, be obtained pure in solution and characterized by high-resolution matrix-assisted laser desorption/ionization mass spectrometry, as well as by ultraviolet–visible and infrared spectroscopy.

Oxidative dimerization of precursors **2b**–**2k** was the final step towards the synthesis of polyynes **1a**–**1j** (Table 2). Standard Hay coupling conditions[18] (CuCl, tetramethylethylenediamine, CH_2Cl_2, O_2) readily converted **2b**–**2d** into tetrayne **1a**, hexayne **1b** and octayne **1c**, respectively. These conditions were not, however, particularly successful when applied to the conversion of **2e** and **2f** into decayne **1d** and dodecayne **1e**, respectively. In these cases, the formation of side products rendered purification and isolation of the desired polyynes difficult. Switching to the typical Eglinton–Galbraith coupling conditions ($Cu(OAc)_2{\cdot}H_2O$, pyridine, THF) gave decayne **1d** and dodecayne **1e** without the troublesome by-products encountered with the Hay protocol, but only in modest isolated yields of 26% and 41%, respectively. By using CH_2Cl_2 as the reaction solvent and the less nucleophilic base 2,6-lutidine, however, the yields of **1d** and **1e** were improved significantly. Gratifyingly, this set of conditions was generally applicable, and terminal polyynes **2g**–**2k** thus provided the remaining members of the series, **1f**–**1j**. The isolated polyynes span a range of colours, starting with tetrayne **1a**, which is colourless. Hexa- and octaynes **1b** and **1c** are both yellow, and decayne **1d** marks the transition from yellow to orange. Polyynes **1e**–**1h** are all isolated as orange solids and the longest derivative, **1j**, is orange–red in colour.

Ultraviolet–visible spectroscopy is a primary tool for polyyne characterization because these molecules typically display well-resolved spectra with distinctive vibrational fine structures[19]. Furthermore, the lowest energy wavelength of significant absorption, λ_{max}, shows a steady shift to lower energy as a function of polyyne length, and this trend documents the lowering of the HOMO → LUMO bandgap energy (E_g) as the conjugation length of the molecule increases. Numerous studies used λ_{max} values for shorter polyynes with n = 2–14 as a predictive tool for carbyne based on the premise that the HOMO → LUMO bandgap should eventually reach an asymptotic limit, which would be a reasonable estimate of λ_{max} (and thus E_g) for carbyne. Typically, a plot of E_g versus $1/n$ was examined (where n is the number of acetylene units) and extrapolation to the y-intercept then provided an estimate of λ_{sat} for an infinite polyyne chain (that is, $\lambda_{sat} = \lambda_{max}$ at the saturation length of the series). For example, this analysis was reported for the series i-Pr_3Si–$[C{\equiv}C]_n$–Sii-Pr_3 (n = 2–10) and predicted a limiting value of λ_{sat} = 570 nm (ref. 20), nearly identical to the value predicted for aryl end-capped polyynes of the same lengths (λ_{sat} = 570 nm)[21]. Similarly, a plot of E_g versus $1/n$ reported for the organometallic series **Pt[*n*]** up to n = 14 predicted a limiting value of λ_{sat} = 573 nm (ref. 11), which is somewhat higher than that determined for an earlier series of Pt-terminated polyynes up to n = 12 ($\lambda_{sat} \approx$ 492–527 nm)[22].

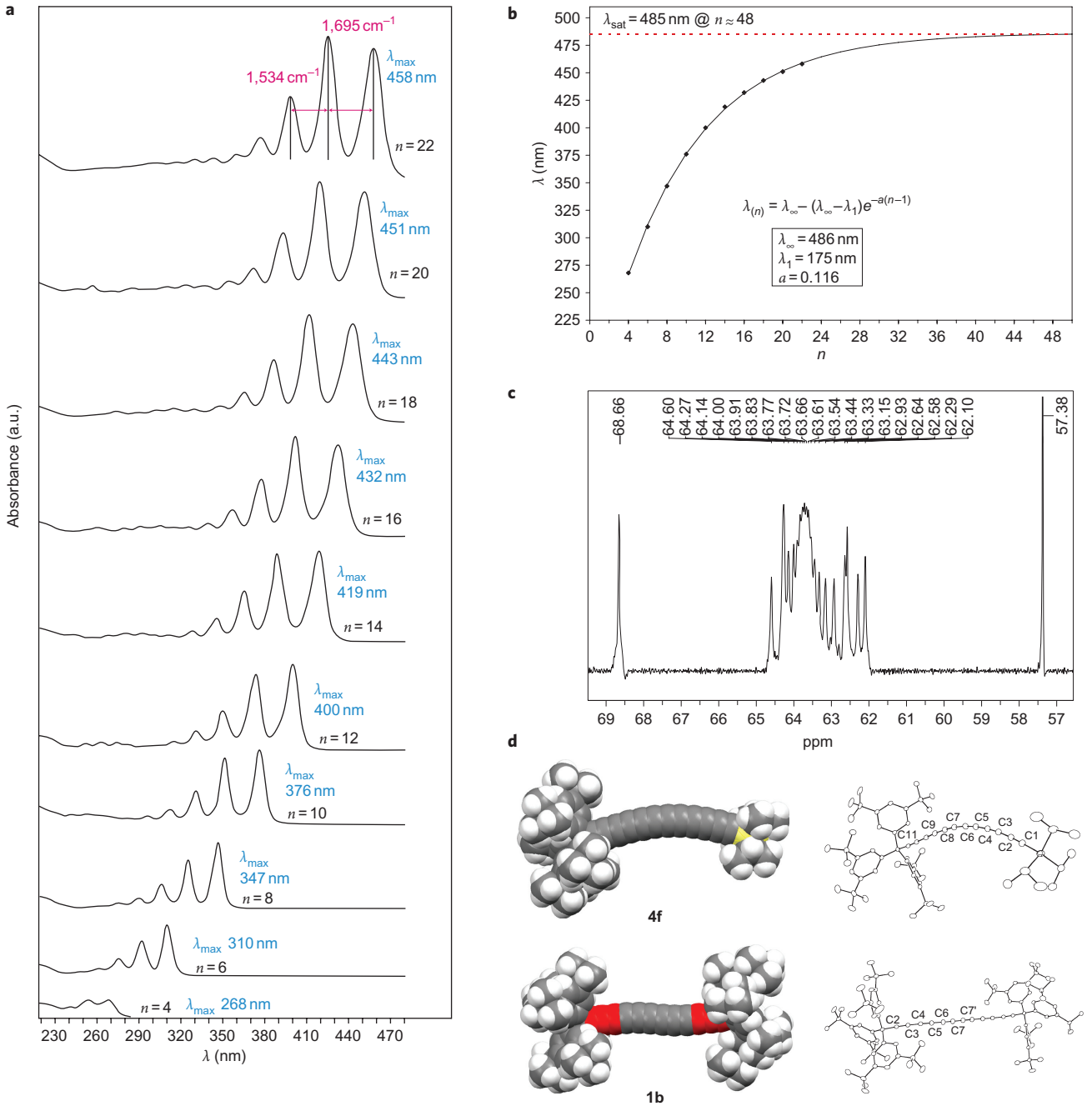

Figure 2 | Spectroscopic and crystallographic characterization of polyynes 1a–1j. a, Ultraviolet–visible spectra of **1a–1j** polyynes as measured in hexanes; wavelength of λ_{max} for each derivative is shown in blue and vibrational separations of lowest energy absorptions for **1j** are shown in magenta. a.u. = arbitrary units. **b**, Convergence of the absorption maxima in the series of **1a–1j** polyynes according to equation (1), where $\lambda_{\infty} = 486$ nm, $\lambda_1 = 175$ nm and $a = 0.116$. **c**, ^{13}C NMR spectrum (in $CDCl_3$) of **1j** in the range 69–57 ppm, which shows convergence of the *sp*-carbon resonances to a median value of ~63.7 ppm (outlying signals at 68.66 and 57.38 ppm arise from the endmost acetylenic carbons). **d**, X-ray crystallographic structures for **4f** and **1b** shown as space-filling models (left) and ORTEP representations (right, 20% probability level, hydrogen atoms not shown); selected bond lengths (Å) for **4f**: C(1)–C(2) 1.213(3), C(2)–C(3) 1.357(4), C(3)–C(4) 1.209(3), C(4)–C(5) 1.360(4), C(5)–C(6) 1.211(3), C(6)–C(7) 1.358(3), C(7)–C(8) 1.202(3), C(8)–C(9) 1.360(4), C(9)–C(10) 1.210(3), C(10)–C(11) 1.364(3), C(11)–C(12) 1.196(3); selected bond lengths (Å) for **1b**: C(2)–C(3) 1.192(3), C(3)–C(4) 1.363(3), C(4)–C(5) 1.205(3), C(5)–C(6) 1.353(3), C(6)–C(7) 1.201(3), C(7)–C(7′) 1.362(5).

The ultraviolet–visible spectra for **1a–1j** are plotted in Fig. 2a, and show the expected vibrational fine structure (for example, spacing of 1,534 and 1,695 cm^{-1} for the three lowest energy absorptions of **1j**). The bathochromic shift in λ_{max} as a function of length spans from $\lambda_{max} = 268$ nm for **1a** to $\lambda_{max} = 458$ nm for **1j**. The extinction coefficients for λ_{max} increase almost uniformly as a function of length with values that approach one million for **1i** ($\varepsilon = 866{,}000$ at $\lambda_{max} = 451$ nm and $\varepsilon = 936{,}000$ at $\lambda = 420$ nm). Following the usual procedure (see above), a plot of the solution optical bandgap E_g versus $1/n$ gave a good fit to the data for series **1a–1j** and predicted a limiting value of $\lambda_{sat} \approx 564$ nm (2.20 eV; see Supplementary Fig. S2). There is, however, a potential problem with this estimation, as previously documented by Meier *et al.* for other rigid, conjugated oligo- and polymers[23]. A plot of E_g versus $1/n$ assumes that E_g continues to decrease uniformly as a function of length through to infinity. It is well-established,

however, that an effective conjugation length (also referred to as a confinement length, convergence length or delocalization length) should exist for π-conjugated organic oligomers. This leads to a convergent limit for properties such as λ_{max} or E_g at lengths much shorter than infinity[24]. Indeed, the plot of E_g versus $1/n$ for series **1** revealed a conspicuous deviation from linearity for the longest members of the series ($n \geq 10$), which suggested a better fit was possible (see Supplementary Fig. S2). Following the Meier protocol[23], the data for series **1a–1j** were analysed using an exponential function (equation (1)).

$$\lambda_{(n)} = \lambda_{\infty} - (\lambda_{\infty} - \lambda_1)e^{-a(n-1)} \quad (1)$$

where n is again the number of acetylene units, $\lambda_{(n)}$ is λ_{max} for a polyyne of length n (λ_1 is thus λ_{max} of the monomer with $n = 1$, calculated according to equation (1)) and λ_{∞} is the limiting value as $n \rightarrow \infty$. The parameter a indicates how fast saturation (convergence) is approached, and it can also be used to compare convergence characteristics between different oligomer series. Finally, a practical definition is required that relates the approach to λ_{∞} and λ_{sat}, and the suggestion of Meier is adopted here[23], taking into account the accuracy of the ultraviolet–visible spectrometer ($\pm$1 nm): λ_{sat} is defined by fulfilment of the relationship $\lambda_{\infty} - \lambda_{(n)} \leq 1$ nm.

Applying the λ_{max} data for **1a–1j** into equation (1) generated the parameters $\lambda_{\infty} = 486 \pm 5$ nm, $\lambda_1 = 175 \pm 13$ nm and $a = 0.116 \pm 0.008$ (for details and error analysis, see Supplementary Table S2). Figure 2b shows the convergence of λ_{max} values for **1a–1j** based on equation (1) and predicts a λ_{sat} for carbyne of 485 nm (2.56 eV) by about $n = 48$. This λ_{sat} value is substantially higher in energy than that predicted by the linear extrapolation method of E_g versus $1/n$ ($\lambda_{sat} \approx 564$ nm, 2.20 eV). Interestingly, the low value of $a = 0.116$ shows that saturation for polyynes was reached quite slowly in comparison to that for other conjugated oligomers, which probably reflects that effective conjugation for polyynes is not dependent on molecular conformation[23]. Given the extensive set of λ_{max} data for polyyne series **1a–1j**, we believe this to be the most accurate estimation to date for the finite HOMO–LUMO gap of carbyne. This analysis also provides excellent evidence that a polyyne structure of alternating single and triple bonds will be maintained for carbyne, that is, Peierls distortion will be upheld[25,26].

All synthesized polyynes **1a–1j** were sufficiently stable and soluble for ^{13}C NMR spectroscopic analysis, which provided additional insight into the prospective properties of carbyne (Table 3). ^{13}C NMR spectroscopy confirmed that the longest member of the series, **1j**, was still a polyyne rather than carbyne; quite amazingly, 21 of the 22 resonances for unique *sp*-carbons were observed (two overlapping signals were found at 64.27 parts per million (ppm)). The two endmost alkyne carbons experienced the greatest influence from the end-capping group and appeared at ~69 and ~57 ppm. The remaining carbon signals resonated within a narrow window of 62.10–64.60 ppm and converged towards a median value of 63.7 ppm (Fig. 2c and Supplementary Fig. S3). Thus, these data suggest that the ^{13}C NMR spectrum of carbyne probably consists of a broadened signal centred at a chemical shift of ~63.7 ppm, a value quite consistent with that expected from a polyynic framework composed of alternating single and triple bonds. This proposed chemical shift is consistent with other predictions[11,20–22], albeit more precise.

X-ray crystallographic analysis of **4f** and **1b** offered an opportunity to examine structural aspects and a means to visualize the steric shielding that results from the presence of the Tr* groups (Fig. 2d). Molecule **4f** adopts a gentle bend in the solid state, and the bond angles for centrosymmetric **1b** show an S-shaped conformation; in both cases the C–C≡C bond angles range from about 175 to 179°. Clearly evident in the structures is the dramatic difference in size between the Tr* (diameter, $d \approx 14$ Å) and *i*-Pr_3Si ($d \approx 7$ Å) groups. Thus, whereas the *i*-Pr_3Si groups do little to shield the polyyne chain, the Tr* groups extend well out over the *sp*-carbon framework, and offer significantly more steric shielding against the prospect of intermolecular interactions that reportedly lead to decomposition (schematically shown in red, Fig. 2d)[9,27,28]. Finally, analysis of bond lengths reveals that C–C and C≡C bonds for both structures remain within the expected ranges[26–28].

Table 3 | ^{13}C NMR alkyne carbon resonances for polyynes 1a–1j.

Compound	Alkyne carbon chemical shifts in $CDCl_3$ (ppm)
1a	69.06, 63.00, 62.36, 57.19
1b	68.78, 62.96, 62.90, 62.75, 62.42, 57.29
1c	68.65, 63.55, 63.49, 62.97, 62.60, 62.50, 62.19, 57.33
1d	68.60, 63.96, 63.78, 63.49, 63.11, 62.69, 62.54, 62.28, 62.06, 57.36
1e	68.57, 64.17, 63.92, 63.77, 63.49, 63.18, 62.86, 62.52, 62.50, 62.17, 61.99, 57.36
1f	68.57, 64.28, 64.00, 63.93, 63.69, 63.45, 63.24, 63.01, 62.74, 62.48, 62.44, 62.12, 61.96, 57.37
1g	68.56, 64.34, 64.05, 64.01, 63.81, 63.61, 63.45, 63.29, 63.12, 62.93, 62.69, 62.48, 62.41, 62.10, 61.95, 57.37
1h	68.55, 64.36, 64.06, 64.04, 63.85, 63.68, 63.55, 63.42, 63.31, 63.19, 63.05, 62.87, 62.65, 62.47, 62.39, 62.08, 61.94, 57.37
1i	68.63, 64.50, 64.19, 64.19, 64.03, 63.88, 63.77, 63.67, 63.58, 63.51, 63.43, 63.33, 63.20, 63.03, 62.81, 62.54, 62.54, 62.20, 62.03, 57.39
1j	68.66, 64.60, 64.27, 64.27, 64.14, 64.00, 63.91, 63.83, 63.77, 63.72, 63.66, 63.61, 63.54, 63.44, 63.33, 63.15, 62.93, 62.64, 62.58, 62.29, 62.10, 57.38

Conclusions

The experimental data reported here are thus consistent with the prediction of carbyne as a polyyne-like material with a structure composed of alternating single and triple bonds with a finite bandgap of $\lambda_{max} = 485$ nm (2.56 eV). The successful synthesis of the longer derivates **1i** and **1j** as persistent molecules is significant, and suggests that longer polyynes, and even carbyne, are viable targets for stepwise synthesis.

Methods

General procedure: modified Eglinton–Galbraith coupling. To a solution of **2** (0.297 mmol) and **3** (1.49 mmol) in CH_2Cl_2 (10 ml), MeOH (10 ml) and 2,6-lutidine (10 ml) was added K_2CO_3 (1.49 mmol) and the mixture was stirred for 10 minutes at room temperature. To the mixture was added $Cu(OAc)_2{\cdot}H_2O$ (2.97 mmol) and the reaction was stirred at room temperature until deemed complete by thin-layer chromatography (TLC) (~17 hours). The reaction was quenched by the addition of saturated aqueous NH_4Cl (25 ml) and the resulting mixture extracted with hexanes (100 ml). The organic phase was washed with saturated aqueous NH_4Cl (25 ml), H_2O (2 × 25 ml) and brine (25 ml), dried over $MgSO_4$ and filtered. The resulting solution was filtered through a plug of silica, the solvent removed *in vacuo* and the crude product purified by column chromatography (silica, hexanes) to yield **4**.

General procedure: desilylation using CsF. To a solution of **4** (1.288 mmol) in THF (100 ml) and H_2O (20 ml) was added CsF (1.54 mmol). The reaction was stirred at room temperature until deemed complete by TLC analysis (~1 hour). The reaction was quenched by the addition of saturated aqueous NH_4Cl (50 ml) and the resulting mixture extracted with hexanes (100 ml). The organic layer was washed with H_2O (50 ml) and brine (50 ml), dried over $MgSO_4$ and filtered. The solvent was removed *in vacuo* and the crude product purified by passing through a plug of silica gel with CH_2Cl_2/hexanes (1:5) to yield **2** ($a = 3$–6).

General procedure: formation of 1f–1j ($n \geq 14$). To a solution of **4** (0.10 mmol) in THF (25 ml) and H_2O (5 ml) was added CsF (0.12 mmol) and the reaction monitored by TLC for completion (~20 minutes). The reaction was quenched by the addition of saturated aqueous NH_4Cl (15 ml) and the resulting mixture extracted with hexanes (50 ml). The organic layer was washed with H_2O (15 ml) and brine (15 ml), dried over $MgSO_4$ and filtered. The resulting solution was concentrated to

~5 ml, and the crude intermediate **2** was passed through a plug of silica gel with CH_2Cl_2/hexanes (1:5). The filtrate was concentrated to ~25 ml and diluted with CH_2Cl_2 (25 ml). $Cu(OAc)_2{\cdot}H_2O$ (0.510 mmol) and 2,6-lutidine (1.0 ml) were added and the reaction mixture was stirred at room temperature for 24 hours. The reaction mixture was concentrated to ~5 ml, the crude product purified by passing through a plug of silica gel with CH_2Cl_2/hexanes (1:10) and the solvent removed *in vacuo* to yield **1**.

Solid-state analyses. Single crystals of **4f** suitable for X-ray crystallographic analysis were grown by slow evaporation of a $CDCl_3$/hexanes (1:1) solution at room temperature. $C_{70}H_{98}Si$, $M_r = 967.57$, triclinic crystal system, space group $P\bar{1}$ (No. 2), $a = 10.2575(7)$ Å, $b = 14.6634(11)$ Å, $c = 21.9595(16)$ Å, $\alpha = 76.520(1)^\circ$, $\beta = 89.555(1)^\circ$, $\gamma = 86.272(1)^\circ$, $V = 3{,}205.0(4)$ Å^3, $Z = 2$, $\rho_{calcd} = 1.003$ g cm^{-3}, $\mu = 0.073$ mm^{-1}, $\lambda = 0.71073$ Å, $T = -100$ °C, $2\theta_{max} = 50.50^\circ$, total data collected = 22,875, $R_1 = 0.0635$ for 6,600 observed reflections with $[F_o^2 \geq 2\sigma(F_o^2)]$, $wR_2 = 0.1884$ for 586 variables and 11,578 unique reflections with $[F_o^2 \geq -3\sigma(F_o^2)]$, residual electron density = 0.407 and −0.258 e Å^{-3}. CCDC no. 772622.

Single crystals of **1b** suitable for X-ray crystallographic analysis were grown by slow evaporation of a xylene solution at room temperature. $C_{98}H_{126}$, $M_r = 1{,}303.99$, triclinic crystal system, space group $P\bar{1}$ (No. 2), $a = 10.5799(10)$ Å, $b = 10.7732(10)$ Å, $c = 19.6616(18)$ Å, $\alpha = 84.7319(14)^\circ$, $\beta = 75.3405(14)^\circ$, $\gamma = 87.4321(14)^\circ$, $V = 2{,}158.4(3)$ Å^3, $Z = 1$, $\rho_{calcd} = 1.003$ g cm^{-3}, $\mu = 0.056$ mm^{-1}, $\lambda = 0.71073$ Å, $T = -100$ °C, $2\theta_{max} = 50.76^\circ$, total data collected = 15,603, $R_1 = 0.0538$ for 4,479 observed reflections with $[F_o^2 \geq 2\sigma(F_o^2)]$, $wR_2 = 0.1535$ for 486 variables and 7,893 unique reflections with $[F_o^2 \geq -3\sigma(F_o^2)]$, residual electron density = 0.408 and −0.195 e Å^{-3}. CCDC no. 772621.

The diameters of the endgroups for **4f** and **1b** were estimated from the radius as measured from the central carbon or silyl atom of the end-capping group to the outermost proton, based on the X-ray crystallographic structures, using Mercury CSD 2.2.

Received 14 April 2010; accepted 27 July 2010; published online 19 September 2010

References

1. Mannion, A. M. *Carbon and its Domestication* (Springer, 2006).
2. Pierson, H. O. *Handbook of Carbon, Graphite, Diamond and Fullerenes – Properties, Processing and Applications* (William Andrew Publishing/Noyes, 1993).
3. Falcao, E. H. L. & Wudl, F. Carbon allotropes: beyond graphite and diamond. *J. Chem. Technol. Biotechnol.* **82,** 524–531 (2007).
4. Webster, A. Carbyne as a possible constituent of the interstellar dust. *Mon. Not. R. Astron. Soc.* **192,** 7–9 (1980).
5. Hayatsu, R., Scott, R. G., Studier, M. H., Lewis, R. S. & Anders, E. Carbynes in meteorites: detection, low-temperature origin, and implications for interstellar molecules. *Science* **209,** 1515–1518 (1980).
6. El Goresy, A. & Donnay, G. A new allotropic form of carbon from the Ries crater. *Science* **161,** 363–364 (1968).
7. Lagow, R. J. *et al.* Synthesis of linear acetylenic carbon: the '*sp*' carbon allotrope. *Science* **267,** 362–367 (1995).
8. Cataldo, F. *Polyynes: Synthesis, Properties and Applications* (Taylor & Francis, 2005).
9. Chalifoux, W. A. & Tykwinski, R. R. Synthesis of extended polyynes: toward carbyne. *C. R. Chim.* **12,** 341–358 (2009).
10. Eastmond, R., Johnson, T. R. & Walton, D. R. M. Silylation as a protective method for terminal alkynes in oxidative couplings. *Tetrahedron* **28,** 4601–4616 (1972).
11. Zheng, Q. *et al.* A synthetic breakthrough into an unanticipated stability regime: a series of isolable complexes in which C_6, C_8, C_{10}, C_{12}, C_{16}, C_{20}, C_{24}, and C_{28} polyynediyl chains span two platinum atoms. *Chem. Eur. J.* **12,** 6486–6505 (2006).
12. Khuong, T.-A. V., Zepeda, G., Ruiz, R., Khan, S. I. & Garcia-Garibay, M. A. Molecular compasses and gyroscopes: engineering molecular crystals with fast internal rotation. *Cryst. Growth Des.* **4,** 15–18 (2004).
13. Jahnke, E. & Tykwinski, R. R. The Fritsch–Buttenberg–Wiechell rearrangement: modern applications for an old reaction. *Chem. Commun.* **46,** 3235–3249 (2010).
14. Eglinton, G. & Galbraith, A. R. Cyclic diynes. *Chem. Ind. (London)* 737–738 (1956).
15. Siemsen, P., Livingston, R. C. & Diederich, F. Acetylenic coupling: a powerful tool in molecular construction. *Angew. Chem. Int. Ed.* **39,** 2633–2657 (2000).
16. Haley, M. M. *et al.* One-pot desilylation/dimerization of ethynyl- and butadiynyltrimethylsilanes. Synthesis of tetrayne-linked dehydrobenzoannulenes. *Tetrahedron Lett.* **38,** 7483–7486 (1997).
17. Wang, C., Batsanov, A. S., West, K. & Bryce, M. R. Synthesis and crystal structures of isolable terminal aryl hexatriyne and octatetrayne derivatives: Ar–$(C{\equiv}C)_n$H (n=3, 4). *Org. Lett.* **10,** 3069–3072 (2008).
18. Hay, A. S. Oxidative coupling of acetylenes II. *J. Org. Chem.* **27,** 3320–3321 (1962).
19. Schermann, G., Grösser, T., Hampel, F. & Hirsch, A. Dicyanopolyynes: a homologous series of end-capped linear *sp* carbon. *Chem. Eur. J.* **3,** 1105–1112 (1997).
20. Eisler, S. *et al.* Polyynes as a model for carbyne: synthesis, physical properties, and nonlinear optical response. *J. Am. Chem. Soc.* **127,** 2666–2676 (2005).
21. Gibtner, T., Hampel, F., Gisselbrecht, J.-P. & Hirsch, A. End-cap stabilized oligoynes: model compounds for the linear *sp* carbon allotrope carbyne. *Chem. Eur. J.* **8,** 408–432 (2002).
22. Mohr, W., Stahl, J., Hampel, F. & Gladysz, J. A. Synthesis, structure, and reactivity of *sp* carbon chains with bis(phosphine) pentafluorophenylplatinum endgroups: butadiynediyl (C_4) through hexadecaoctaynediyl (C_{16}) bridges, and beyond. *Chem. Eur. J.* **9,** 3324–3340 (2003).
23. Meier, H., Stalmach, U. & Kolshorn, H. Effective conjugation length and UV/vis spectra of oligomers. *Acta Polym.* **48,** 379–384 (1997).
24. Martin, R. E. & Diederich, F. Linear monodisperse π-conjugated oligomers: model compounds for polymers and more. *Angew. Chem. Int. Ed.* **38,** 1350–1377 (1999).
25. Hoffmann, R. How chemistry and physics meet in the solid state. *Angew. Chem. Int. Ed.* **26,** 846–878 (1987).
26. Chalifoux, W. A., McDonald, R., Ferguson, M. J. & Tykwinski, R. R. *tert*-Butyl-end-capped polyynes: crystallographic evidence of reduced bond-length alternation. *Angew. Chem. Int. Ed.* **48,** 7915–7919 (2009).
27. Szafert, S. & Gladysz, J. A. Carbon in one dimension: structural analysis of the higher conjugated polyynes. *Chem. Rev.* **103,** 4175–4205 (2003).
28. Szafert, S. & Gladysz, J. A. Update 1 of: Carbon in one dimension: structural analysis of the higher conjugated polyynes. *Chem. Rev.* **106,** PR1–PR33 (2006).

Acknowledgements

This work was supported by the University of Alberta and the Natural Sciences and Engineering Research Council of Canada (NSERC) through the Discovery Grant program. W.A.C. thanks the NSERC (Postgraduate Scholarship-D) and the Alberta Ingenuity Fund for scholarship support. We also thank F. Marsiglio for discussions and M. Ferguson and R. McDonald for solving the X-ray structures for **4f** and **1b**, respectively.

Author contributions

W.A.C. designed the experiments, and performed the syntheses, characterization and property studies. W.A.C. and R.R.T co-wrote the paper. R.R.T conceived the project.

Additional information

The authors declare no competing financial interests. Supplementary information and chemical compound information accompany this paper at www.nature.com/naturechemistry. Reprints and permission information is available online at http://npg.nature.com/reprintsandpermissions/. Correspondence and requests for materials should be addressed to R.R.T.